Thiophene-fused aromatic belts

Hiroki Shudo[1], Philipp Wiesener[2], Elena Kolodzeiski[3], Kiichi Mizukami[4], Harry Mönig[2,*], Saeed Amirjalayer[3,*], Hirotoshi Sakamoto[5], Henning Klaasen[6], Bart Jan Ravoo[6], Nobuo Kimizuka[4,*], Akiko Yagi[1,7,*], and Kenichiro Itami[7,8,*]

[1] Department of Chemistry, Graduate School of Science, Nagoya University; Chikusa, Nagoya 464-8602, Japan.

[2] Institute of Physics, University of Münster; Münster 48149, Germany.

[3] TUM School of Natural Sciences, Department of Chemistry, Technical University of Munich; München 85748, Germany.

[4] Graduate School of Engineering, Kyushu University; Fukuoka 819-0395, Japan.

[5] Institute for Integrated Cell-Material Sciences (WPI-iCeMS), Kyoto University; Kyoto 606-8501, Japan.

[6] Organic-Chemistry Institute, University of Münster; Münster 48149, Germany.

[7] Institute of Transformative Bio-Molecules (WPI-ITbM); Nagoya University, Chikusa, Nagoya 464-8602, Japan.

[8] Molecule Creation Laboratory, RIKEN Cluster for Pioneering Research, RIKEN; Wako, Saitama 351-0198, Japan.

*Email: harry.moenig@uni-muenster.de (H.M.), s.amirjalayer@uni-muenster.de (S.A.), kimizuka.nobuo.763@m.kyushu-u.ac.jp (N.K.), yagi.akiko@itbm.nagoya-u.ac.jp (A.Y.), kenichiro.itami@riken.jp (K.I.)

nanobelt chemistry

**thiophene-fused aromatic belt
(thiophene belt)**

thiophene chemistry
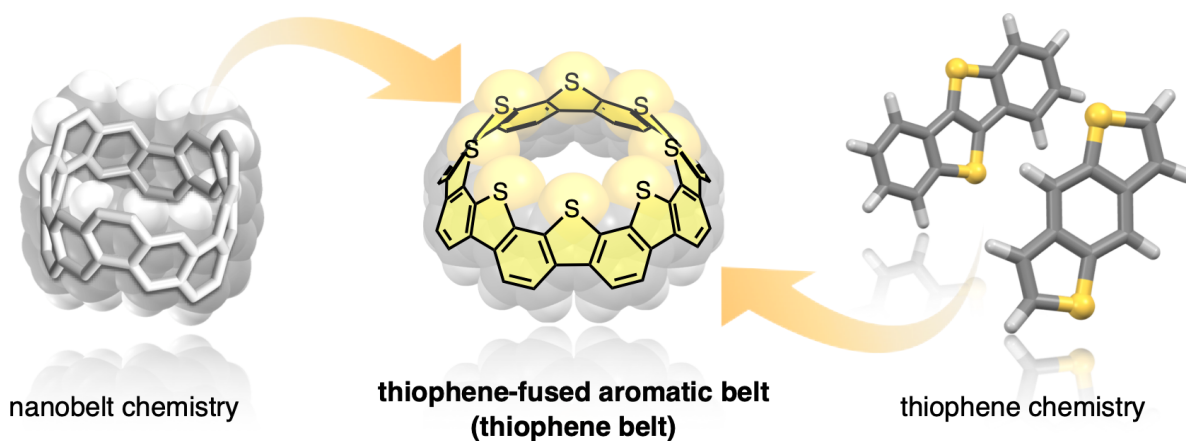
Abstract:

Aromatic belts, ultrashort carbon nanotubes and related structures, are emerging molecular entities in the fields of organic electronics and supramolecular chemistry owing to their structural rigidity, fully fused π-conjugation, and well-defined cavity. Synthesis of aromatic belts with embedded thiophene structures, which manifest significant optoelectronic and conductive properties, has not yet been achieved. Herein, we report the synthesis of long sought-after thiophene-fused aromatic belts (thiophene belts) via one-step sulfur cross-linking reaction of partially fluorinated cycloparaphenylenes. Their unique structural features, including unidirectional columnar stacking with high dipole moment in crystals, two-dimensional layer assembly on metal surfaces, and unique photophysical properties, such as long-lifetime phosphorescence, were uncovered. These distinctive features of the thiophene belts should inspire a range of applications such as next-generation optoelectronic devices and polar materials.

Introduction

Aromatic belts, molecules comprising aromatic rings connected in tubular structures, have been of interest to theoretical chemists as well as synthetic and physical chemists for over 70 years owing to their uniquely rigid tubular structures and associated electronic properties.[1-5] Stimulated by our first synthesis of a (6,6)carbon nanobelt in 2017,[6] many research groups have successfully synthesized a range of carbon nanobelts and related aromatic belts.[3,7-12] Most importantly, it has inspired chemists to apply sophisticated synthetic strategies[3,5] to access aromatic belts that were previously considered impossible to synthesize due to their high strain energies. Aromatic nanobelts are emerging as a new enterprise in chemistry. Their rigid and hollow structures, which can be regarded as ultrashort carbon nanotubes, are expected to have a variety of applications, such as host-guest chemistry and optoelectronic materials.[2,3,13,14] Importantly, Zang et al. demonstrated that nanobelts have high conductance in single-molecule devices, highlighting the importance of radial π-conjugation for high conductivity.[14] When considering applications in the field of organic electronics, there are many reasons for investigating and incorporating fused thiophenes, which are known to be multifunctional and monopolistic core structures. As representatives of electron-donating π-electron systems, fused thiophenes are widely used as the basic backbone of p-type organic semiconductors, molecular conductors, and light-emitting materials.[15-18] Therefore, the synthesis of aromatic belts that incorporate fused thiophenes should lead to the provision of nanobelts with new functions. Herein, we report the synthesis of long sought-after thiophene-fused aromatic belts (thiophene belts) via one-step sulfur cross-linking of partially fluorinated cycloparaphenylenes (CPPs) (Figure 1A). The unique structural features, photophysical properties, and alignment on the metal surfaces were also elucidated in this study. These features of the thiophene belts have inspired a range of applications in various fields.

Results and discussion

Structure prediction and synthesis of thiophene belts

Before investigating the synthesis of thiophene belts, strain energy calculations were performed at the B3LYP/6-31G(d) level of theory to understand their structural properties. The strain energy was calculated using a hypothetical homodesmotic reaction (Figure 1B).[19] When the diameter is small (n = 6–18; n indicates the number of thiophene units), the thiophene belts adopt cone-shaped structures with a strain energy behavior similar to that of previously reported nanobelts. Thiophene belts are most stable in flattened structures when their diameter exceeds a certain threshold (n = 18–26). In the larger thiophene belts (n = 28–36), the shapes are the same as those of the saddle-shaped surfaces. The change in shape with an increasing number of repeating units is similar to that of sulflowers[20] or cyclothiophenes.[21-23]

3
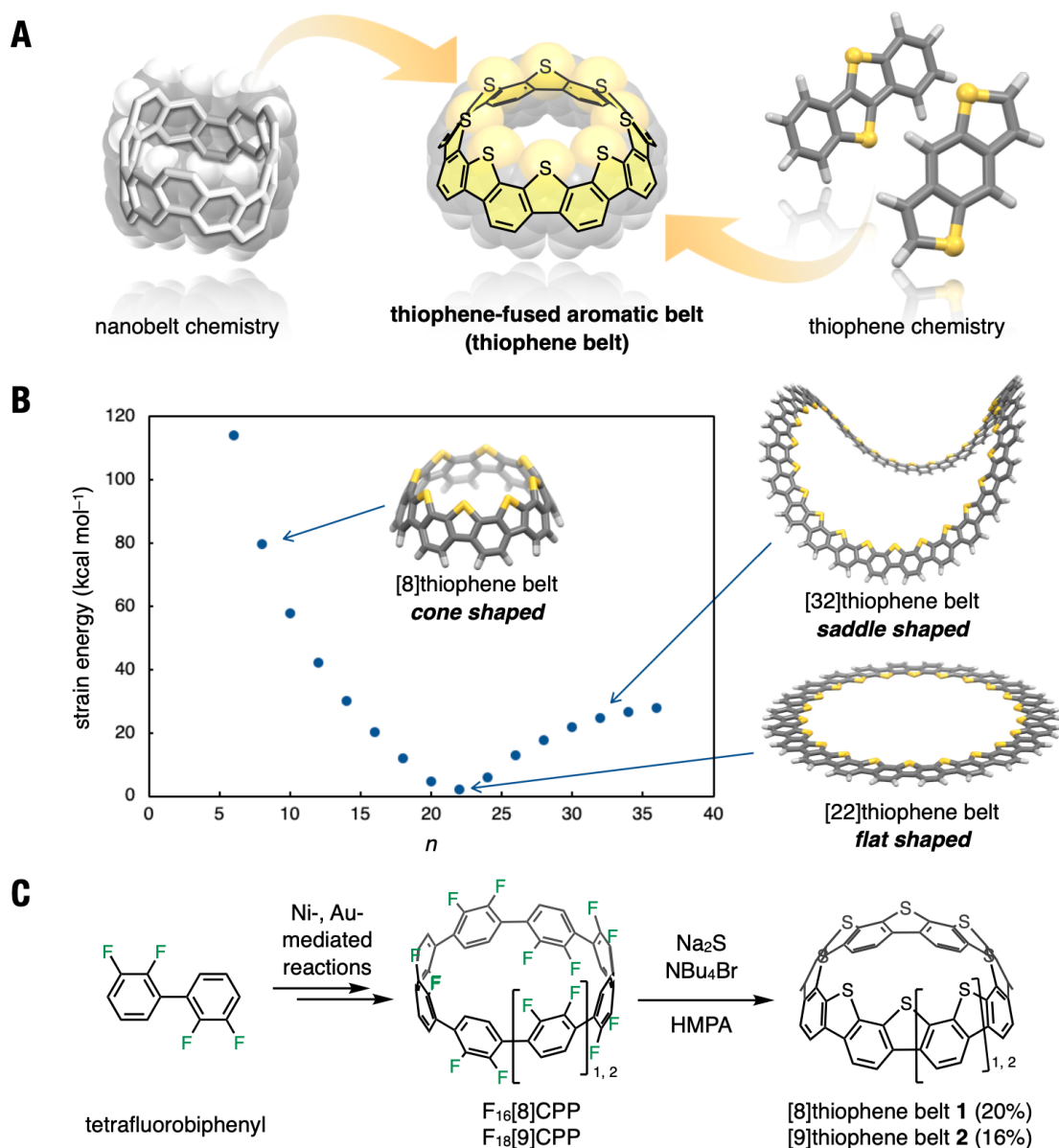
Figure 1. Strain energies, predicted structures, and synthesis of thiophene belts. (**A**) Fusion of nanobelt chemistry and thiophene chemistry. (**B**) Plotting strain energies versus n (number of benzene rings) and cone-shaped (n = 6–18), flat-shaped (n = 18–26), and saddle-shaped structures (n = 28–36) of thiophene belts. (**C**) Scheme for the syntheses of thiophene belts **1** and **2**. Na_2S, sodium sulfide; NBu_4Br, tetrabutylammonium bromide; HMPA, hexamethylphosphoric triamide.

In this study, cone-shaped thiophene belts were synthesized (Figure 1C). Among various theoretical approaches, we envisioned a ring-to-belt synthesis through the late-stage sulfur-embedding reaction of a CPP core.[24-26] Thus, significant strain energy gain is not required during the difficult belt-forming events.[5] For the C–S bond formation, we chose nucleophilic aromatic substitution (S_NAr) reactions at the C–F bonds because of their reliability and simplicity.[27] Thus, [8]thiophene belt (**1**) and [9]thiophene belt (**2**) were synthesized from the corresponding half-fluorinated CPPs, F_{16}[8]CPP and F_{18}[9]CPP. Following extensive investigations, we found that the starting materials (F_{16}[8]CPP and F_{18}[9]CPP) can be synthesized via our nickel-based method[28,29] and Tsuchido's gold-

4

based method[30,31] from readily available 2,2',3,3'-tetrafluorobiphenyl. Details of the synthesis are provided in Supporting Information. For key sulfur-embedding S_NAr reactions, the conditions reported by Amsharov are particularly effective.[32] Thus, a mixture of F_{16}[8]CPP (1.0 equiv), sodium sulfide (80 equiv.), and tetrabutylammonium bromide (TBAB: 16 equiv.) in hexamethylphosphoric triamide (HMPA) was heated at 180 °C for 3 h under microwave irradiation. Following purification by precipitation, washing, and silica gel chromatography, the [8]thiophene belt (**1**) was successfully isolated in 20% yield as a stable yellow solid (Figure 1C). Under similar S_NAr reaction conditions, F_{18}[9]CPP was converted to [9]thiophene belt (**2**) in 16% isolated yield (Figure 1C). Despite the large number of reaction points (16 C–F bonds for **1**, 18 C–F bonds for **2**), both reactions proceeded with approximately 90% efficiency per C–F bond. However, because F_{12}[6]CPP[29] did not tolerate the reaction conditions, [6]thiophene belt was not obtained.

In the ^{1}H NMR spectra of **1** and **2**, only singlet signals were observed in both cases (see Supporting Information for details). Structural optimization by density functional theory (DFT) calculations resulted in structures with high symmetry of C_{8v} for **1** and C_{9v} for **2**. The results of NMR analysis and calculations suggest that the thiophene belts have high symmetry, even in solution. The NMR signals of hydrogen atoms in the thiophene belts were found to be of a lower magnetic field shifted than that of CPP (**1**: 7.72 ppm, [8]CPP: 7.48 ppm, **2**: 7.85 ppm, [9]CPP: 7.52 ppm, see Supporting Information for details).[26,33] This can be interpreted as a result of the stronger anti-shielding effect of hydrogen atoms owing to the belt-like structural constraint of the CPP backbone by sulfur cross-linking.

Crystal structures and packing of thiophene belts

Suitable single crystals of **1** and **2** were obtained from solutions of dichloromethane for **1** and chlorobenzene for **2**, respectively. Their structures were successfully determined using X-ray crystallography. As shown in Figure 2A, **1** and **2** adopt belt-shaped and truncated conical structures (C_{8v} and C_{9v} symmetries, respectively). These unique shapes result from a structure in which only one side of the CPP backbone is cross-linked with sulfur atoms. The taper angles of the conical structures in each thiophene belt are 50° for **1** and 58° for **2**, respectively. Consistent with the DFT calculation results, the angle increases with increasing belt size. The measured diameters of the inscribed and circumscribed circles in the observed structures of thiophene belts are 8.67 Å and 12.9 Å for **1**, 9.75 Å and 14.2 Å for **2**, respectively (Figure 2A and B, center and right). Another interesting feature of thiophene belts is that they are neutral, yet significantly polar molecules because the sulfur atoms are clustered on one side of the belts. According to DFT calculations at the B3LYP/6-31G(d) level of theory, the electrostatic potential map shows that the negative potential density is concentrated on the sulfur side. In addition, **1** has a dipole moment of 8.19 Debye and **2** has that of 8.87 Debye. The results show that polarity increases with the increasing number of sulfur atoms with the cone-shaped nanobelt structures (Figure 2E, see Supporting Information for details).

5
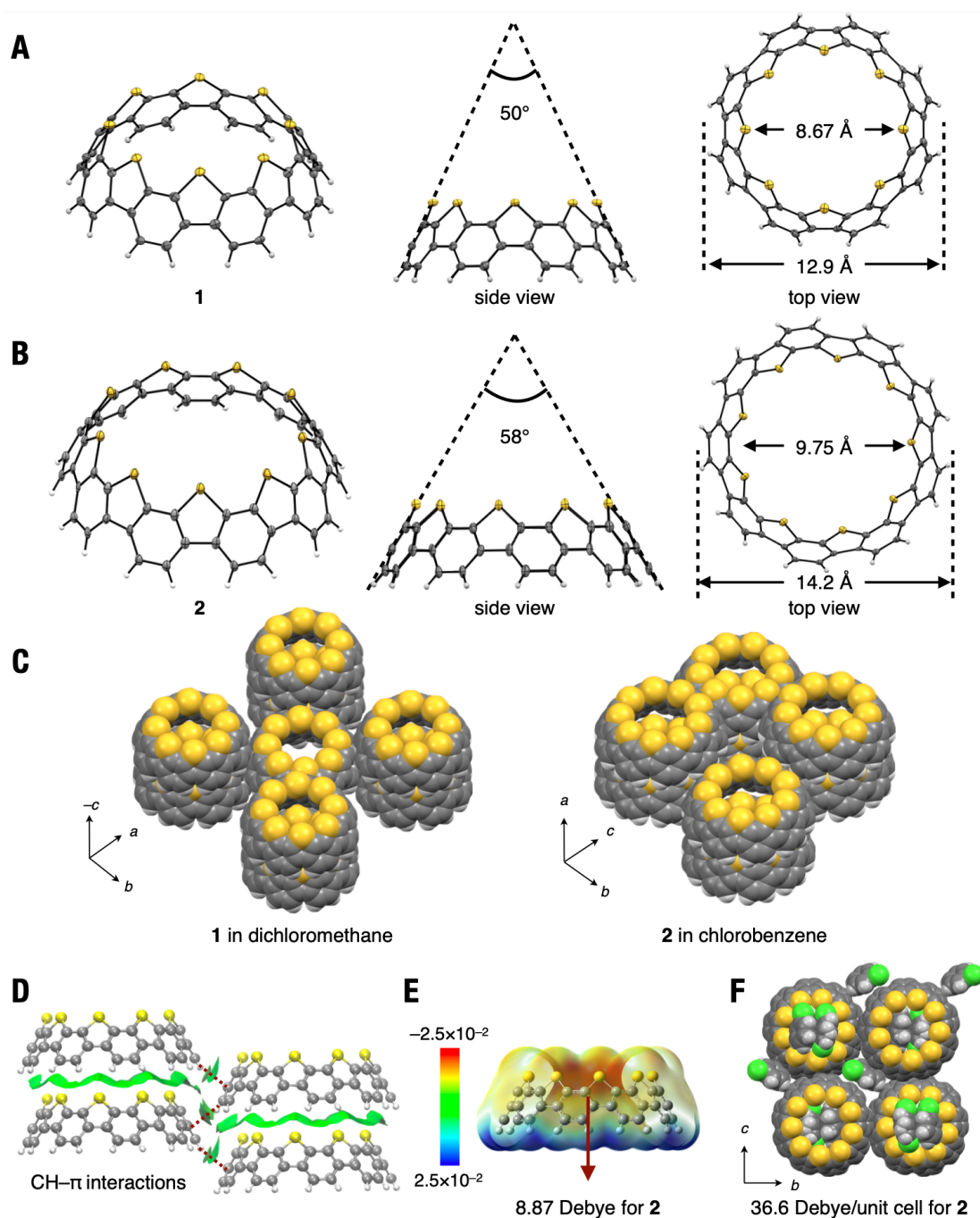
Figure 2. Structural features of thiophene belts. (**A** and **B**) The Oak Ridge thermal-ellipsoid plot (ORTEP) drawings of **1** and **2** with thermal ellipsoids at 50% probability (**A** for **1**, **B** for **2**, center: side views and taper angles, right: top views, diameters of inscribed circle and circumscribed circle). Solvent molecules are omitted for clarity. (**C**) Packing structures of **1** and **2**. Solvent molecules (dichloromethane for the left, and chlorobenzene for the right) are omitted for clarity. (**D**) Non-covalent interaction (NCI) plot of **2** visualizing intramolecular interactions using X-ray structure. An isosurface value of 0.30 a.u. is applied to the structure. (**E**) Electrostatic surface potential maps calculated for **2** with isovalues plotted at 0.001 and the value of dipole moment for **2**. (**F**) Unit cell structure for **2** and the value of dipole moment per unit cell.

Despite the use of thiophene belts of various sizes and different solvents to prepare the crystals, all packing structures for **1** and **2** were stacked in a columnar manner (Figure 2C, left: dichloromethane for **1**, and right: chlorobenzene for **2**, benzene/pentane and

6

chloroform/pentane for **1**: see Supporting Information for details). Since certain bowl-shaped molecules are known to form columnar stacks,[34-38] the conical structures of the thiophene belts may stabilize columnar packing, as visualized by the non-covalent interaction (NCI) plot (Figure 2D). Interestingly, because each column is oriented in the same direction, the crystals of the thiophene belts provide space with broken spatial symmetry (Figure 2C). In the case of thiophene belts, all adjacent columns in the crystals of **1** and **2** are not perfectly parallel but are aligned with a half-molecular translation of the thiophene belt. Non-polar assemblies are often advantageous because the antiparallel orientation of the dipoles in each column is more electrostatically favorable than the parallel orientation.[34] The intermolecular distance between columns is 2.73 Å for **2**, which corresponds to the CH–π interaction (Figure 2D). The packing of thiophene belts can efficiently generate CH–π interactions like herringbone due to the inclination of the conical structures. The calculations also show that the crystals, including the solvent in **2**, are polar crystals (36.6 Debye per unit cell, Figure 2F). Polar materials and single crystals are of significant interest owing to their unique properties such as ferroelectricity and the bulk photovoltaic effect.[34,35,39-43] Moreover, this remarkable column-forming tendency of the thiophene belts was observed in the just-evaporated sample of **2** supported by the powder X-ray diffraction pattern (see Supporting Information for details). The tubular space surrounded by sulfur atoms, given by the characteristic structure of the belt, has no similar examples. These features, coupled with manifesting one-dimensional and parallel-orienting polar assemblies, stimulate the use of thiophene belts for various optoelectronic applications.

Photophysical properties of thiophene belts

Optical measurements and DFT calculations were performed to investigate the optoelectronic properties of thiophene belts. The ultraviolet–visible (UV–vis) absorption of dichloromethane solutions of **1** and **2** exhibit absorption peaks at 345 nm and 351 nm, respectively (Figure 3A, solid green and blue lines, respectively). In the case of **1**, the peak top is red-shifted compared to that of pristine [8]CPP ([8]CPP: 339 nm) and blue-shifted compared to that of methylene-bridged [8]cycloparaphenylene ([8]MCPP: 388 nm),[44] which has a rigid CPP moiety similar to **1**. In the case of **2**, the top of the peak is slightly red-shifted from that of pristine [9]CPP (340 nm), as in the case of **1**. The absorption edges of **1** and **2** are observed at approximately 470 and 450 nm, respectively. Time-dependent (TD)-DFT calculations at the B3LYP/6-31G(d) level revealed the transitions attributable to each peak (see Supporting Information for details). The highest occupied molecular orbital (HOMO) and lowest unoccupied molecular orbital (LUMO) of **1** reflect the fused structure of cyclothiophenes[21-23] and CPPs[45] whereas HOMO and HOMO–1 reflect the isoelectronic structure[17] of cyclophenacene, which is an unsynthesized aromatic belt (Figure 3B, see Supporting Information for details).[2,3]

7
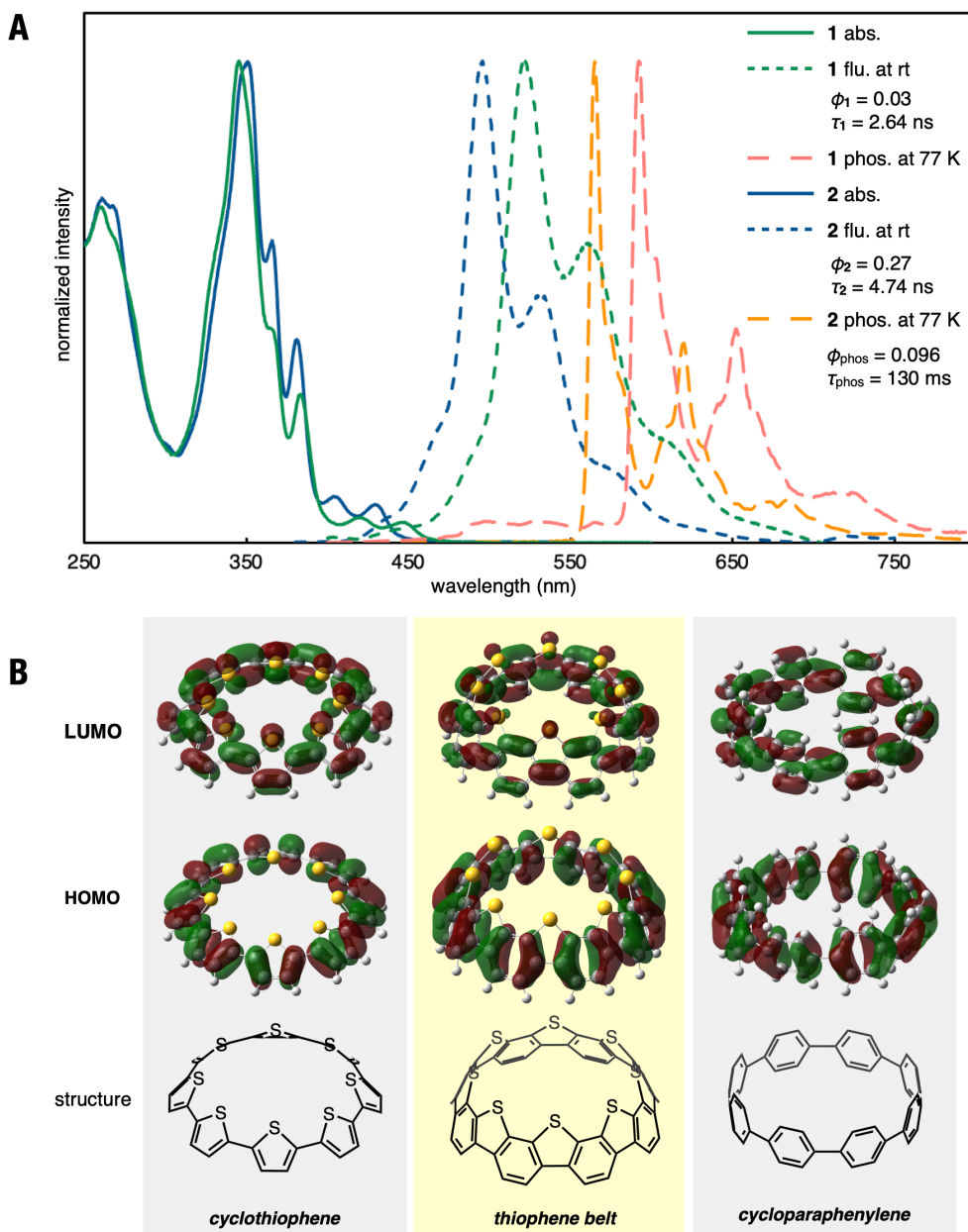
Figure 3. Photophysical properties of thiophene belts. (**A**) Ultraviolet–visible absorption and fluorescence spectra of the diluted dichloromethane solution of thiophene belts at room temperature (abs: solid lines, flu: dashed lines, green for **1** and blue for **2**). The fluorescence quantum yield and lifetime are shown in the upper right corner. Phosphorescence spectra of thiophene belts in 2-methyltetrahydrofuran at 77 K upon excitation at 350 nm (long dashed lines, pink for **1** and orange for **2**). The phosphorescence quantum yield and lifetime for **2** are shown in the upper right corner. (**B**) Structures and frontier molecular orbitals calculated at the B3LYP/6-31G(d) level of theory (isovalue: 0.02) of **1** (yellow square), cyclothiophene (left gray square), and cycloparaphenylene (right gray square) of the same ring-size as **1**. Green and red indicate negative and positive wave functions, respectively; HOMO, highest occupied molecular orbital; LUMO, lowest unoccupied molecular orbital. HOMO and LUMO of **1** reflect the fused structure of cyclothiophene and cycloparaphenylene.

In the fluorescence measurements, dichloromethane solutions of **1** and **2** exhibit fluorescence with peaks at 521 nm for **1** and 496 nm for **2** (Figure 3A, dashed green and blue lines). The maximum fluorescence wavelength of **1** is blue-shifted compared to those

of [8]CPP and [8]MCPP ([8]CPP: 541 nm, [8]MCPP: 592 nm).[44] While no vibrational structures were observed in the fluorescence of the pristine CPPs, vibrational structures were observed in the thiophene belts, most likely because of their rigid structures. Nanobelts **1** and **2** exhibit fluorescence quantum yield (Φ_F) of 0.03 and 0.27, respectively, the latter being smaller than that observed for [9]CPP (Φ_F = 0.73, Figure S8 in Supporting Information). The observed lower Φ_F for **2**, despite the more rigid structure, can be attributed to the strong spin-orbit coupling (SOC) exhibited by the sulfur atom.[46] The fluorescence lifetimes of the thiophene belts were estimated to be 2.64 ns for **1** and 4.74 ns for **2**, respectively. According to the equations $\Phi_F = k_r \times \tau$ and $k_r + k_{nr} = \tau^{-1}$, the radiative (k_r) and nonradiative (k_{nr}) decay rate constants from the singlet excited state are determined as $k_r = 1.1 \times 10^7$ s^{-1}; $k_{nr} = 3.7 \times 10^8$ s^{-1} for **1**, $k_r = 5.7 \times 10^7$ s^{-1}; $k_{nr} = 1.5 \times 10^8$ s^{-1} for **2**.

Importantly, phosphorescence was observed at low temperature (77 K). The phosphorescence spectra of 2-methyltetrahydrofuran solutions of **1** and **2** exhibit peaks at 592 and 565 nm, respectively, corresponding to vibrational structures (Figure 3A, dashed orange and pink lines). The phosphorescence of **1** could not exclude the minor peak on the short-wavelength side of the major peak, owing to unremovable trace amounts of impurities. The phosphorescence spectra of thiophene belts are considerably blue-shifted compared to those of CPPs, and the size dependency is consistent with the behavior of the phosphorescence spectra of CPPs ([8]CPP: 671 nm, [9]CPP: 633 nm).[47] The phosphorescence quantum yield (Φ_{phos}) for **2** is 0.096. The phosphorescence lifetimes of the thiophene belts were also measured (Figure 3A, see Supporting Information for details). Long-lifetime phosphorescence was observed in one component for **2** (τ_{phos} =130 ms). The phosphorescence lifetimes of the thiophene belts are more than 1000 times longer than those of CPPs ([8]CPP: 0.060 ms, [9]CPP: 0.063 ms).[47] Usually, in π-conjugated molecules, high-frequency vibrational modes inevitably accelerate nonradiative deactivation.[48] The long phosphorescence lifetime observed in **2** compared to that of [9]CPP may be due to the rigid sulfur-bridged belt structure, which reduces the number of C–H bonds and their stretch modes, suppressing vibrational deactivation. Nevertheless, the observed long-lived excited triplet states are of interest as this feature is essential in the emerging fields of triplet-triplet annihilation upconversion[49] and photo-induced dynamic nuclear polarization.[50]

Assembly of thiophene belts on metal surfaces

The synthesized thiophene belts are defined by all sulfur atoms pointing in the same direction, resulting in a high dipole moment. To investigate how this dipole and the metal-sulfur interactions influence the nucleation of these molecular tubes on metal surfaces, scanning tunneling microscopy (STM) in conjunction with DFT simulations was performed. Therefore, belt **1** was deposited on the Au(111) and Cu(111) surfaces by sublimation at a deposition temperature of 350 °C. Adsorbed single molecules can be identified straightforwardly by their distinct circular contrast in constant current STM, which further

proves a successful synthesis and deposition of the thiophene belts. Imaging at a bias voltage of 2 V, the diameter of the ring can be estimated to be 8.3 Å, which matches the calculated size of **1** (see Supporting Information for details). On the Au(111) surface, **1** is predominantly nucleated at the step edges at low coverages (Figure 4A). In contrast, on the Cu(111) surface, islands of self-assembled thiophene belts were observed in a two-dimensional densely ordered packing (Figure 4D). The measurements suggest that the observed assemblies are of single-molecular height on both the Au and Cu surfaces and that there is no stacking at these coverages (see Supporting Information for details). Generally, pristine CPPs decompose at high temperatures owing to their high strain energies. Therefore, previously reported STM images of the CPP derivatives were prepared using the drop-cast method.[51] As shown by the present measurements, **1** withstood sublimation temperatures as high as 350 °C, which suggests that the linking of the CPP scaffold with sulfur atoms significantly increases the stability of **1**.
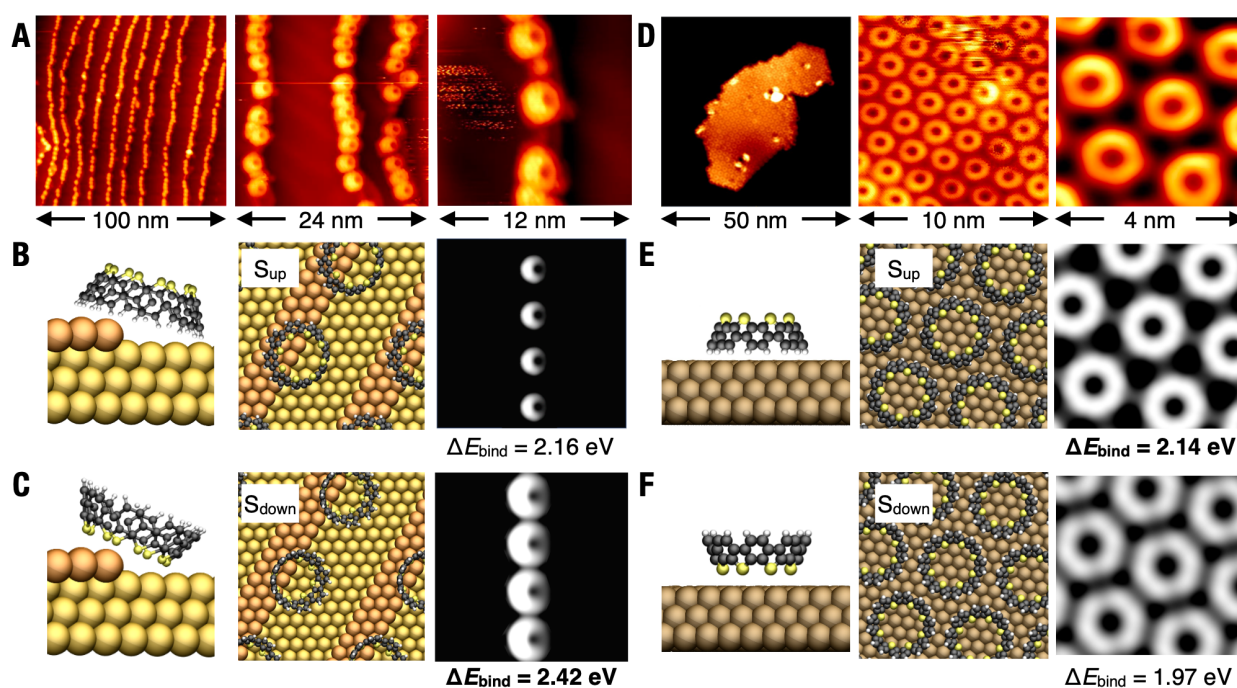
Figure 4. Scanning tunneling microscopy (STM) images of **1** and theoretical simulations of STM. (**A**) STM image of **1** on the Au(111) surface (Bias voltage 2 V, Setpoint current 10 pA). Image in the range of 100 nm, 24 nm, and 12 nm, respectively. (**B** and **C**) Schematic of **1** with sulfur atoms facing up for **B**, and sulfur atoms facing down for **C**. Top view of geometry-optimized facing up or down (center of **B** and **C**, respectively) **1** as self-assembly on Au surface. Simulated STM image and binding energy with sulfur atoms facing up and down (right of **B** and **C**, respectively). (**D**) STM image of **1** on the Cu(111) surface (Bias voltage 2 V, Setpoint current 10 pA). Image in the range of 50 nm, 10 nm, and 4 nm, respectively. (**E** and **F**) Schematic of **1** with sulfur atoms facing up for **E** and sulfur atoms facing down for **F**. Geometry-optimized top view of facing up or down (center of **E** and **F**, respectively) **1** as self-assembly on Cu surface. Simulated STM image and binding energy with sulfur atoms facing up and down (right of **E** and **F**, respectively).

https://doi.org/10.26434/chemrxiv-2024-zllzl ORCID: https://orcid.org/0000-0001-5227-7894 Content not peer-reviewed by ChemRxiv. License: CC BY-NC-ND 4.0

To clarify whether the sulfur atoms of **1** face up or down on the metal surfaces, DFT calculations and STM simulations were performed using the Vienna Ab Initio Simulation Package (VASP)[52,53] (Figure 4B, C, E, and F). On the Au(111) surface, the structure with sulfur atoms facing down toward the Au step edges is in better agreement with the measured data of the STM images, whereas on the Cu(111) surface, the structure with sulfur atoms facing up toward the Cu surface shows better agreement. Furthermore, the binding energies of **1** under upward- and downward-facing sulfur atoms on both Au and Cu surfaces were calculated. On the Au(111) surface, the calculations emphasize that conformations with sulfur contacts pointing toward the metal step edges are preferred ($\Delta E_{bind,S\text{-}up}$ = 2.16 eV and $\Delta E_{bind,S\text{-}down}$ = 2.42 eV; Figure 4B and C). Remarkably, the experiments on Au(111) further show that the thiophene belts exclusively show a stable binding conformation at the step edges, while on flat terraces they are more mobile and agglomerate in small islands in a disordered manner (see Supporting Information for details). In contrast, on the Cu(111) surface, the calculations show that the thiophene belt **1** is preferentially aligned with sulfur atoms facing up ($\Delta E_{bind,S\text{-}up}$ = 2.14 eV and $\Delta E_{bind,S\text{-}down}$ = 1.97 eV; Figure 4, E and F), favoring a conformation that enables multiple points of contact (16 C–H bonds) with the metal surface. Therefore, the molecules are more stable on the Cu(111) surface and arrange in ordered islands. In conclusion, the preferred orientation of the thiophene belt may depend on the interaction format of each type of metal.

Conclusions

Thiophene belts with a merged structure of recently emerging aromatic belts and function-rich fused thiophenes have been successfully synthesized via sulfur-embedding ring-to-belt transformations. The established synthetic routes to thiophene belts (**1** and **2**) are reasonably short-step from readily available 2,2',3,3'-tetrafluorobiphenyl (two steps for **1** and five steps for **2**). Their unique structural features, such as unidirectional columnar stacking with high dipole moment in crystals as well as in a just-evaporated sample, and metal-dependent assembly on Au(111) and Cu(111) surfaces, as well as unique photophysical properties, such as long-lifetime phosphorescence, were uncovered. In the context of rather independent yet very exciting developments of aromatic belts and fused thiophenes in the fields of structural organic chemistry and organic electronics, the "merged" molecules (thiophene belts) with significantly unique properties discovered in this study have the potential to stimulate a range of applications in various fields, such as single-molecule electronics, supramolecular materials, photovoltaics, and triplet-triplet annihilation upconversion. While we demonstrated the synthesis of cone-shaped thiophene belts in this study, we believe that the present ring-to-belt transformation strategy would enable access to other thiophene belts with different topologies as well as other heteroatom-embedded aromatic belts. These synthetic and application-oriented campaigns will lead to significant breakthroughs in the science and technology of aromatic belts.

Supporting Information:

Materials and methods, experimental procedures, photophysical studies, NMR spectra, and computational details are available in the Supporting Information or from the corresponding authors upon request. The crystallographic data for compounds **1** and **2** are available free of charge from the Cambridge Crystallographic Data Centre under CCDC identifiers 2373105–2373107 (www.ccdc.cam.ac.uk/structures/). STM simulations have been carried out using computational and data resources provided by the Leibniz Supercomputing Center (www.lrz.de).

Author contributions:

H.Sh., A.Y., and K.I. conceived the concept. K.I. directed the project. H.Sh. synthesized compounds **1** and **2** and performed DFT calculations. H.Sh. performed X-ray crystallography. H.Sh. and K.M. performed the photophysical measurements. H.Sh. K.M. and N.K. analyzed the photophysical properties of **1** and **2**. P.W. and H.M. performed STM measurements. E.K. and S.A. performed the periodic DFT calculations and STM simulations on the metal substrates. H.Sh. and H.Sa. performed the XRD measurements. H.Sh. and H.K. measured the evaporation temperature without molecular decomposition. H.Sh., A.Y., and K.I. wrote the manuscript with feedback from other authors. All authors approved the final version of the manuscript.

Competing interests:

The authors declare no conflict of interest. No patents were filed.

References

1. E. Heilbronner, Molecular Orbitals in homologen Reihen mehrkerniger aromatischer Kohlenwasserstoffe: I. Die Eigenwerte yon LCAO-MO's in homologen Reihen. *Helv. Chim. Acta* **1954**, *37*, 921–935.

2. Q. H. Guo, Y. Qiu, M. X. Wang, J. F. Stoddart, Aromatic hydrocarbon belts. *Nat. Chem.* **2021**, *13*, 402–419.

3. D. Imoto, A. Yagi, K. Itami, Carbon Nanobelts: Brief History and Perspective. *Precis. Chem.* **2023**, *1*, 516–523.

4. G. R. Schaller, R. Herges, "Aromatic Belts as Sections of Nanotubes" in *Fragments of Fullerenes and Carbon Nanotubes: Designed Synthesis, Unusual Reactions, and Coordination Chemistry*, M. A. Petrukhina, L. T. Scott Eds. (Wiley, 2011), pp. 259–258.

5. K. Y. Cheung, Y. Segawa, K. Itami, Synthetic Strategies of Carbon Nanobelts and Related Belt-Shaped Polycyclic Aromatic Hydrocarbons. *Chem. Eur. J.* **2020**, *65*, 14791–14801.

6. G. Povie, Y. Segawa, T. Nishihara, Y. Miyauchi, K. Itami, Synthesis of a carbon nanobelt. *Science* **2017**, *356*, 172–175.

7. K. Y. Cheung, S. Gui, C. Deng, H. Liang, Z. Xia, Z. Liu, L. Chi, Q. Miao, Synthesis of Armchair and Chiral Carbon Nanobelts. *Chem* **2019**, *5*, 838–847.

8. K. Y. Cheung, K. Watanabe, Y. Segawa, K. Itami, Synthesis of a zigzag carbon nanobelt. *Nat. Chem.* **2021**, *13*, 255–259.

9. Y. Han, S. Dong, J. Shao, W. Fan, C. Chi, Synthesis of a Sidewall Fragment of a (12,0) Carbon Nanotube. *Angew. Chem. Int. Ed.* **2021**, *60*, 2658–2662.

10. Z. Xia, S. H. Pun, H. Chen, Q. Miao, Synthesis of Zigzag Carbon Nanobelts through Scholl Reactions. *Angew. Chem. Int. Ed.* **2021**, *60*, 10311–10318.

11. Y. Segawa, T. Watanabe, K. Yamanoue, M. Kuwayama, K. Watanabe, J. Pirillo, Y. Hijikata, K. Itami, Synthesis of a Möbius carbon nanobelt. *Nat. Synth.* **2022**, *1*, 535–541.

12. W. Fan, T. M. Fukunaga, S. Wu, Y. Han, Q. Zhou, J. Wang, Z. Li, X. Hou, H. Wei, Y. Ni, H. Isobe, J. Wu, Synthesis and chiral resolution of a triply twisted Möbius carbon nanobelt. *Nat. Synth.* **2023**, *2*, 880–887.

13. M. Yamashina, Y. Tanaka, R. Lavendomme, T. K. Ronson, M. Pittelkow, J. R. Nitschke, An antiaromatic-walled nanospace. *Nature* **2019**, *574*, 511–515.

14. J. Lin, S. Wang, F. Zhang, B. Yang, P. Du, C. Chen, Y. Zang, D. Zhu, Highly efficient charge transport across carbon nanobelts. *Sci. Adv.* **2022**, *8*, eade4692.

15. I. F. Perepichka, D. F. Perepichka, Eds., *Handbook of Thiophene-Based Materials: Applications in Organic Electronics and Photonics* (Wiley, 2009).

16. A. Mishra, C. Q. Ma, P. Bäuerle, Functional Oligothiophenes: Molecular Design for Multidimensional Nanoarchitectures and Their Applications. *Chem. Rev.* **2009**, *109*, 1141–1276.

17. K. Takimiya, S. Shinamura, I. Osaka, E. Miyazaki, Thienoacene-Based Organic Semiconductors. *Adv. Mater.* **2011**, *38*, 4347–4370.

18. F. A. Larik, M. Faisal, A. Saeed, Q. Abbas, M. A. Kazi, N. Abbas, A. A. Thebo, D. M. Khan, P. A. Channar, Thiophene-based molecular and polymeric semiconductors for organic field effect transistors and organic thin film transistors. *J. Mater. Sci.: Mater. Electron.* **2018**, *29*, 17975–18010.

19. Y. Segawa, H. Omachi, K. Itami, Theoretical Studies on the Structures and Strain Energies of Cycloparaphenylenes. *Org. Lett.* **2010**, *12*, 2262–2265.

20. K. Yu. Chernichenko, V. V. Sumerin, R. V. Shpanchenko, E. S. Balenkova, V. G. Nenajdenko, "Sulflower": A New Form of Carbon Sulfide. *Angew. Chem. Int. Ed.* **2006**, *45*, 7367–7370.

21. J. Krömer, I. Rios-Carreras, G. Fuhrmann, C. Musch, M. Wunderlin, T. Debaerdemaeker, E. Mena-Osteritz, P. Bäuerle, Synthesis of the First Fully α-Conjugated Macrocyclic Oligothiophenes: Cyclo[*n*]thiophenes with Tunable Cavities in the Nanometer Regime. *Angew. Chem. Int. Ed.* **2000**, *39*, 3481–3486.

22. F. Zhang, G. Götz, H. D. F. Winkler, C. A. Schalley, P. Bäuerle, Giant Cyclo[*n*]thiophenes with Extended π Conjugation. *Angew. Chem. Int. Ed.* **2009**, *48*, 6632–6635.

23. S. S. Zade, M. Bendikov, Cyclic Oligothiophenes: Novel Organic Materials and Models for Polythiophene. A Theoretical Study. *J. Org. Chem.* **2006**, *71*, 2972–2981.

24. R. Jasti, J. Bhattacharjee, J. B. Neaton, C. R. Bertozzi, Synthesis, Characterization, and Theory of [9]-, [12]-, and [18]Cycloparaphenylene: Carbon Nanohoop Structures. *J. Am. Chem. Soc.* **2008**, *52*, 17646–17647.

25. H. Takaba, H. Omachi, Y. Yamamoto, J. Bouffard, K. Itami, Selective Synthesis of [12]Cycloparaphenylene. *Angew. Chem. Int. Ed.* **2009**, *48*, 6112–6116.

26. S. Yamago, Y. Watanabe, T. Iwamoto, Synthesis of [8]Cycloparaphenylene from a Square-Shaped Tetranuclear Platinum Complex. *Angew. Chem. Int. Ed.* **2010**, *49*, 757–759.

27. A. A. Kamin, T. D. Clayton, C. E. Otteson, P. M. Gannon, S. Krajewski, W. Kaminsky, R. Jasti, D. J. Xiao, Synthesis and metalation of polycatechol nanohoops derived from fluorocycloparaphenylenes. *Chem. Sci.* **2023**, *14*, 9724–9732.

28. H. Shudo, M. Kuwayama, M. Shimasaki, T. Nishihara, Y. Takeda, N. Mitoma, T. Kuwabara, A. Yagi, Y. Segawa, K. Itami, Perfluorocycloparaphenylenes. *Nat. Commun.* **2022**, *13*, 3713.

29. H. Shudo, M. Kuwayama, Y. Segawa, A. Yagi, K. Itami, Half-substituted fluorocycloparaphenylenes with high symmetry: synthesis, properties and derivatization to densely substituted carbon nanorings. *Chem. Commun.* **2023**, *59*, 13494–13497.

30. Y. Tsuchido, R. Abe, T. Ide, K. Osakada, A Macrocyclic Gold(I)–Biphenylene Complex: Triangular Molecular Structure with Twisted Au_2(diphosphine) Corners and Reductive Elimination of [6]Cycloparaphenylene. *Angew. Chem. Int. Ed.* **2020**, *59*, 22928–22932.

31. Y. Yoshigoe, Y. Tanji, Y. Hata, K. Osakada, S. Saito, E. Kayahara, S. Yamago, Y. Tsuchido, H. Kawai, Dynamic Au–C σ-Bonds Leading to an Efficient Synthesis of [*n*]Cycloparaphenylenes (*n* = 9–15) by Self-Assembly. *JACS Au* **2022**, *2*, 1857–1868.

32. M. Feofanov, V. Akhmetov, R. Takayama, K. Y. Amsharov, Facile Synthesis of Thienoacenes via Transition-Metal-Free Ladderization. *J. Org. Chem.* **2021**, *86*, 14759–14766.

33. Y. Segawa, P. Šenel, S. Matsuura, H. Omachi, K. Itami, [9]Cycloparaphenylene: Nickel-mediated Synthesis and Crystal Structure. *Chem. Lett.* **2011**, *40*, 423–425.

34. C. Zhang, Y. Guo, D. He, J. Komiya, G. Watanabe, T. Ogaki, C. Wang, A. Nihonyanagi, H. Inuzuka, H. Gong, Y. Yi, K. Takimiya, D. Hashizume, D. Miyajima, A Design Principle for Polar Assemblies with C_3-Sym Bowl-Shaped π-Conjugated Molecules. *Angew. Chem. Int. Ed.* **2021**, *60*, 3261–3267.

35. S. Furukawa, J. Y. Wu, M. Koyama, K. Hayashi, N. Hoshino, T. Takeda, Y. Suzuki, J. Kawamata, M. Saito, T. Akutagawa, Ferroelectric columnar assemblies from the bowl-to-bowl inversion of aromatic cores. *Nat. Commun.* **2021**, *12*, 768.

36. T. Amaya, S. Seki, T. Moriuchi, K. Nakamoto, T. Nakata, H. Sakane, A. Saeki, S. Tagawa, T. Hirao, Anisotropic Electron Transport Properties in Sumanene Crystal. *J. Am. Chem. Soc.* **2009**, *131*, 408–409.

37. X. Lu, T. Y. Gopalakrishna, Y. Han, Y. Ni, Y. Zou, J. Wu, Bowl-Shaped Carbon Nanobelts Showing Size-Dependent Properties and Selective Encapsulation of C_{70}. *J. Am. Chem. Soc.* **2019**, *141*, 5934–5941.

38. Z.-L. Qiu, Y. Cheng, Q. Zeng, Q. Wu, X.-J. Zhao, R.-J. Xie, L. Feng, K. Liu, Y.-Z. Tan, Synthesis and Interlayer Assembly of a Graphenic Bowl with Peripheral Selenium Annulation. *J. Am. Chem. Soc.* **2023**, *145*, 3289–3293.

39. K. T. Butler, J. M. Frost, A. Walsh, Ferroelectric materials for solar energy conversion: photoferroics revisited. *Energy Environ. Sci.* **2015**, *8*, 838–848.

40. S. Horiuchi, Y. Tokunaga, G. Giovannetti, S. Picozzi, H. Itoh, R. Shimano, R. Kumai, Y. Tokura, Above-room-temperature ferroelectricity in a single-component molecular crystal. *Nature* **2010**, *463*, 789–793.

41. D. Miyajima, F. Araoka, H. Takazoe, J. Kim, K. Kato, M. Takata, T. Aida, Ferroelectric Columnar Liquid Crystal Featuring Confined Polar Groups Within Core-Shell Architecture. *Science* **2012**, *336*, 209–213.

42. A. S. Tayi, A. K. Shveyd, A. C.-H. Sue, J. M. Szarko, B. S. Rolczynski, D. Cao, T. J. Kennedy, A. A. Sarjeant, C. L. Stern, W. F. Paxon, W. Wu, S. K. Dey, A. C. Fahrenbach, J. R. Guest, H. Mohseni, L. X. Chen, K. L. Wang, J. F. Stoddart, S. I. Stupp, Room-temperature ferroelectricity in supramolecular networks of charge-transfer complexes. *Nature* **2012**, *488*, 485–489.

43. R. K. Vijayaraghaven, S. C. J. Meskers, M. A. Rahim, S. Das, Bulk photovoltaic effect in an organic polar crystal. *Chem. Commun.* **2014**, *50*, 6530–6533.

44. H. Kono, Y. Li, R. Zanasi, G. Monaco, F. F. Summa, L. T. Scott, A. Yagi, K. Itami, Methylene-Bridged [6]-, [8]-, and [10]Cycloparaphenylenes: Size-Dependent Properties and Paratropic Belt Currents. *J. Am. Chem. Soc.* **2023**, *145*, 8939–8946.

45. Y. Segawa, A. Fukazawa, S. Matsuura, H. Omachi, S. Yamaguchi, S. Irle, K. Itami, Combined experimental and theoretical studies on the photophysical properties of cycloparaphenylenes. *Org. Biomol. Chem.* **2012**, *10*, 5979–5984.

46. S.-Y. Yang, Y.-K. Wang, C.-C. Peng, Z.-G. Wu, S. Yuan, Y.-J. Yu, H. Li, T.-T. Wang, H.-C. Li, Y.-X. Zheng, Z.-Q. Jiang, L.-S. Liao, Circularly Polarized Thermally Activated Delayed Fluorescence Emitters in Through-Space Charge Transfer on Asymmetric Spiro Skeletons. *J. Am. Chem. Soc.* **2020**, *142*, 17756–17765.

47. M. Fujitsuka, C. Lu, T. Iwamoto, E. Kayahara, S. Yamago, T. Majima, Properties of Triplet-Excited [*n*]Cycloparaphenylenes (*n* = 8–12): Excitation Energies Lower than Those of Linear Oligomers and Polymers. *J. Phys. Chem. A* **2014**, *118*, 4527–4532.

48. P. Ghosh, A. M. Alvertis, R. Chowdhury, P. Murto, A. J. Gillett, S. Dong, A. J. Sneyd, H.-H. Cho, E. W. Evans, B. Monserrat, F. Li, C. Schnedermann, H. Bronstein, R. H. Friend, A. Rao, Decoupling excitons from high-frequency vibrations in organic molecules. *Nature* **2024**, *629*, 355–362.

49. S. E. Seo, H.-S. Choe, H. Cho, H. Kim, J.-H. Kim, O. S. Kwon, Recent advances in materials for and applications of triplet–triplet annihilation-based upconversion. *J. Mater. Chem. C* **2022**, *10*, 4483–4496.

50. K. Nishimura, H. Kouno, Y. Kawashima, K. Orihashi, S. Fujiwara, K. Tateishi, T. Uesaka, N. Kimizuka, N. Yanai, Materials chemistry of triplet dynamic nuclear polarization. *Chem. Commun.* **2020**, *56*, 7217–7232.

51. D. Lu, H. Wu, Y. Dai, H. Shi, X. Shao, S. Yang, J. Yang, P. Du, A cycloparaphenylene nanoring with graphenic hexabenzocoronene sidewalls. *Chem. Commun.* **2016**, *52*, 7164–7167.

52. G. Kresse, J. Furthmüller, Efficient iterative schemes for *ab initio* total-energy calculations using a plane-wave basis set. *Phys. Rev. B* **1996**, *54*, 11169–11186.

53. G. Kresse, J. Furthmüller, Efficiency of ab-initio total energy calculations for metals and semiconductors using a plane-wave basis set. *Comput. Mater. Sci.* **1996**, *6*, 15–50.